A Computational Model for Single Iron Particle Combustion in Liquid-Phase

Aki Fujinawa, Joel Jean-Philyppe, Jeffrey M. Bergthorson
Department of Mechanical Engineering, McGill University
Montreal, Quebec, Canada

XiaoCheng Mi
Department of Mechanical Engineering, Eindhoven University of Technology
5600 MB, Eindhoven, the Netherlands

1 Introduction

Iron, given its carbon-free nature and high energy density [1, 2], is an ideal candidate as a clean and efficient energy carrier that can store and transport renewable energy. While the solid-phase ignition process of an iron particle is well understood [3, 4], the many outstanding unknowns of iron oxidation lie in temperatures where iron and its oxide products exist in liquid-phase. A number of recent studies have focused on single particle combustion [5–8], however, no extensive quantitative analysis on the internal kinetics of a burning molten droplet, or the composition of such a droplet was made. Although further experimental campaigns are necessary to fully elucidate the governing physics of iron particle combustion in liquid-phase, reasonable inferences can be made to model the process approximately. It is known that condensed-phase kinetics of iron oxidation are sufficiently fast such that at elevated temperatures (i.e., when the iron particle becomes fully molten at $T_{\mathrm{p}} = 1870$ K), the rate of liquid-phase iron oxidation should be limited by the external-oxidizer-transport rate [4]. While there is no quantitative information on the composition of a reactive molten droplet of iron, higher oxidized species such as Fe_3O_4 and Fe_2O_3 are not thermodynamically favored at elevated temperatures, and wüstite (FeO) is most likely the only stable product during the initial liquid-phase burn of an iron particle. The current work presents the framework of a computational model for the liquid-phase combustion of a single iron particle, based on the simplifying assumptions that the rate of external oxidizer transport is rate limiting, and FeO is the predominant oxide species that initially forms in liquid-phase.

2 Model for iron particle combustion

2 Solid-phase oxidation and solid-to-liquid phase transition

The model for solid-phase oxidation is largely based on the work of Mi *et al.* [4], as illustrated in Fig. 1 (a). The kinetic rate of oxide layer growth is modified to consider the shrinking-core effect, and the

maximum oxygen transport rate to the particle surface is modified to consider the effect of Stefan flow via the equation $\dot{m}_{O_2,\max} = -4\pi r_p \mathcal{D}_{O_2} \rho \ln(1 - Y_{O_2,\infty})$. Between 1650 K and 1870 K, the phase transition of FeO ($T_{\text{melt}} = 1650$ K), Fe ($T_{\text{melt}} = 1809$ K), and Fe_3O_4 ($T_{\text{melt}} = 1870$ K) occur. To capture these processes, once the melting point of species i is reached, the increase in particle enthalpy is tracked such that the particle remains at the phase-transition temperature until the latent heat of fusion of species i has been overcome.

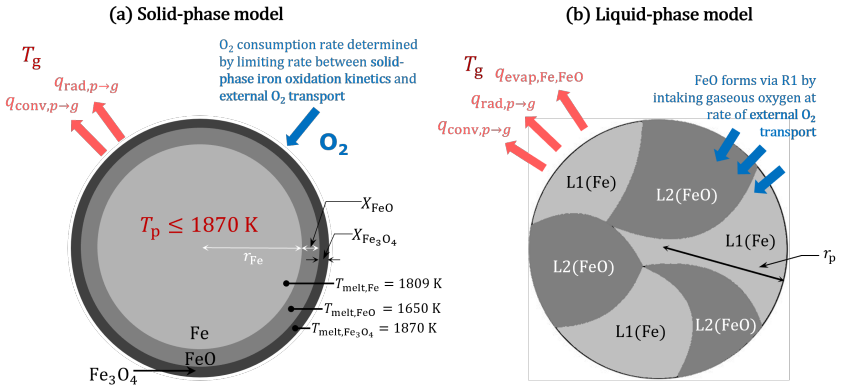

Figure 1: The thermophysical model of a (a) solid-phase iron particle in a layer-by-layer structure and a (b) mixed molten droplet of Fe and FeO in liquid-phase.

2 Model formulation for a single molten droplet

The model for the liquid-phase combustion considers a mixed spherical droplet consisting of L1 (molten Fe) and L2 (molten FeO), each randomly distributed within the particle and covering the particle surface as illustrated in Fig. 1 (b). The formation of liquid-phase FeO is considered, following the reaction R1:

$$\text{R1}: \ \text{Fe}(\ell) + \frac{1}{2}\text{O}_2(\text{g}) \rightarrow \text{FeO}(\ell). \qquad (1)$$

The internal kinetics governing the formation of liquid-phase FeO is assumed to be sufficiently rapid, such that the reaction R1 progresses at the rate of external O_2 transport from the bulk gas to the particle surface. Once the melting point of Fe_3O_4 (1870 K) is reached, and the simulation is stopped.

The evaporation of Fe and FeO are considered, and are described by the reactions R2 and R3 [9],

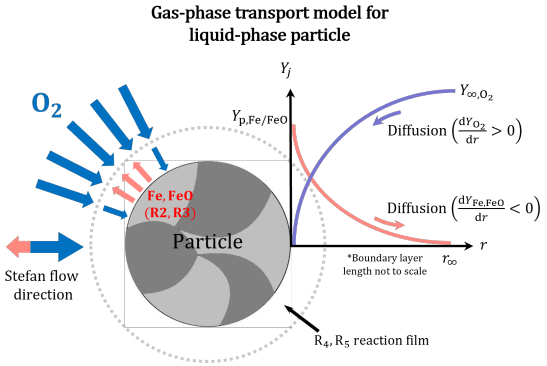

Figure 2: Schematic describing gas-phase transport through the boundary layer in the vicinity of the particle surface, where O_2 diffuses to the particle surface, and Fe and FeO diffuse away from the particle surface due to evaporation, and a bulk transport of the gas occurs due to Stefan flow.

$$\text{R2}: \text{Fe(c)} \leftrightarrow \text{Fe(g)}, \qquad (2)$$

$$\text{R3}: \text{FeO(c)} \leftrightarrow \text{FeO(g)}, \qquad (3)$$

where letters c and g denote condensed-phase and gas-phase, respectively. These evaporation reactions are resolved in the gas-transport model, as illustrated in Fig. 2. The vapor pressures of the dissociative evaporation of FeO and Fe_3O_4 are significantly lower than that of the evaporation of Fe and the non-dissociative evaporation of FeO at temperatures between 2000 and 3000 K, hence, the dissociative evaporation reactions are neglected. The outward transported gas-phase Fe and FeO are considered to readily oxidize and condense into FeO and Fe_3O_4 respectively, by instantaneously consuming inward-transported O_2 to the particle via the reactions R4 and R5:

$$\mathrm{R4} : \mathrm{Fe(g)} + \frac{1}{2}\mathrm{O_2(g)} \leftrightarrow \mathrm{FeO(c)} \tag{4}$$

$$\mathrm{R5} : \mathrm{3FeO(g)} + \frac{1}{2}\mathrm{O_2(g)} \leftrightarrow \mathrm{Fe_3O_4(c)}. \tag{5}$$

The reactions R4 and R5 inhibit the formation of condensed-phase FeO in the particle by consuming inward transported O_2. The gas-phase enthalpy is not tracked, as the heat release associated with the vapor-phase reactions around a single particle is negligible compared to the bulk heat capacity of the gas-phase environment.

2.1 Mass and energy balance equations

The formation rate of FeO via R1 is expressed as follows:

$$\frac{\mathrm{d}m_{\mathrm{FeO,form}}}{\mathrm{d}t} = \nu_{\mathrm{FeO/O_2,c}}(\dot{m}_{\mathrm{O_2}} - \nu_{\mathrm{O_2/Fe,g}}\dot{m}_{\mathrm{Fe}} - \nu_{\mathrm{O_2/FeO,g}}\dot{m}_{\mathrm{FeO}}). \tag{6}$$

The mass balance equations for Fe and FeO during the liquid-phase combustion are written as follows:

$$\frac{\mathrm{d}m_{\mathrm{Fe}}}{\mathrm{d}t} = -\nu_{\mathrm{Fe/FeO,c}}\frac{\mathrm{d}m_{\mathrm{FeO,form}}}{\mathrm{d}t} - \dot{m}_{\mathrm{Fe}} \tag{7}$$

$$\frac{\mathrm{d}m_{\mathrm{FeO}}}{\mathrm{d}t} = \frac{\mathrm{d}m_{\mathrm{FeO,form}}}{\mathrm{d}t} - \dot{m}_{\mathrm{FeO}}. \tag{8}$$

The variables $\nu_{\mathrm{Fe/FeO,c}}$ and $\nu_{\mathrm{FeO/O_2,c}}$ denote the stoichiometric mass ratios for the condensed-phase reaction R1, while the variables $\nu_{\mathrm{O_2/Fe,g}}$ and $\nu_{\mathrm{O_2/FeO,g}}$ denote the stoichiometric mass ratios for the gas-phase reactions R4 and R5, respectively. The variables $\dot{m}_{\mathrm{O_2}}$, $\dot{m}_{\mathrm{Fe}}$, and $\dot{m}_{\mathrm{FeO}}$ each denote the mass transport rate of gas-phase O_2, Fe, and FeO, due to combined diffusion and Stefan flow transport. The O_2 transport-limited formation rate of FeO is inhibited by the stoichiometric consumption of gas-phase O_2 by the outward-transported gas-phase Fe and FeO.

The total enthalpy of the particle H_{p} is calculated as the sum of the enthalpy of each condensed-phase species, expressed as $H_{\mathrm{p}} = \sum_j^{N_{\mathrm{s}}} \frac{m_j h_j(T_{\mathrm{p}})}{M_j}$, where N_{s} is the total number of species, m_{j} is the mass of the j^{th} species, h_j is the molar enthalpy of the j^{th} species as a function of particle temperature T_{p} calculated using the NASA 7-coefficient polynomial parametrization [10], and M_{j} is the molecular weight of the j^{th} species. With the particle enthalpy H_{p} and species masses m_j known, the particle temperature can be determined via a root-finding iterative scheme.

The particle enthalpy evolves according to the rate of addition of the enthalpy due to the incorporated oxygen, heat loss rate due to the heat exchange with the surrounding gas via convection and radiation, and heat absorption (loss) rate due to the evaporation of condensed-phase iron and iron oxide species:

$$\frac{\mathrm{d}H_{\mathrm{p}}}{\mathrm{d}t} = -\frac{h_{\mathrm{O_2}}}{M_{\mathrm{O_2}}}\frac{\mathrm{d}m_{\mathrm{O_2}}}{\mathrm{d}t} - A_{\mathrm{p}}[h_{\mathrm{p}}(T_{\mathrm{p}} - T_{\mathrm{g}}) + \epsilon\sigma(T_{\mathrm{p}}^4 - T_{\mathrm{g}}^4)] - L_{\mathrm{Fe,v}}\dot{m}_{\mathrm{Fe}} - L_{\mathrm{FeO,v}}\dot{m}_{\mathrm{FeO}}. \tag{9}$$

Note that explicit formulations of the heat release associated with the formation of oxide products are not included in Eqn. 9, since the computation of the total particle enthalpy in Eqn. **??** takes into account the heat of formation of species. The first term on the right-hand side of Eqn. 9 describes the addition of the enthalpy of oxygen consumed by the particle. The molar enthalpy of oxygen, h_{O_2}, is calculated using polynomials given by the NASA polynomials [10]. The convective heat transfer coefficient, h_{p}, can be calculated as $h_{\mathrm{p}} = \frac{\mathrm{Nu}\lambda_{\mathrm{g}}}{D_{\mathrm{p}}}$, where Nu and D_{p} are the Nusselt number and diameter of the particle, respectively. For a spherical particle in quiescent gas, the expression simplifies to $h_{\mathrm{p}} = \lambda_{\mathrm{g}}/r_{\mathrm{p}}$. The mixture-averaged gas-phase thermal conductivity λ_{g} is calculated as a function of the gas temperature in the vicinity of the particle surface T_{sf}, using the NASA polynomials [10]. The symbols ϵ and σ in the radiative heat transfer term denote the emissivity of the particle and the Stefan-Boltzmann constant, respectively. Here, the emissivity the molten droplet is taken as 0.7 [11] (as opposed to 0.88 in solid-phase [4, 12]), as the outer surface of the molten droplet consists of L2 phase. The last two terms on the right-hand side of Eqn. 9 describe the heat absorption due to the evaporation of Fe and FeO, where the constants $L_{\mathrm{Fe,v}}$ and $L_{\mathrm{FeO,v}}$ denote the latent heat of vaporization of Fe and FeO, respectively.

2.2 Gas-phase transport

As illustrated in Fig. 2, evaporated Fe and FeO diffuse outward from the particle, O_2 diffuses inward to the particle, and the bulk gas is transported in the direction of the overall Stefan velocity. The model assumes quasi-steady mass transport and constant thermophysical property values of 2/3 law-averaged temperature, pressure, and gas-composition. For a spherically-symmetric boundary layer, the conservation of mass is $\frac{\mathrm{d}}{\mathrm{d}r}(\rho_{\mathrm{g}} r^2 u) = 0$, where ρ_{g} is the gas density and u is the Stefan velocity. The Stefan velocity is equivalent to the aggregate velocity induced by mass transport rate of O_2, Fe and FeO. The conservation of mass simplifies to the following:

$$\rho_{\mathrm{g}} r^2 u = \mathrm{const.} = \frac{\dot{m}_{\mathrm{O}_2} + \dot{m}_{\mathrm{Fe}} + \dot{m}_{\mathrm{FeO}}}{4\pi}. \tag{10}$$

The gas phase conservation equation for the mass fraction of transported species j is as follows:

$$\frac{\mathrm{d}}{\mathrm{d}r}(\rho_{\mathrm{g}} r^2 u Y_j) - \frac{\mathrm{d}}{\mathrm{d}r}(\rho_{\mathrm{g}} D_j r^2 \frac{\mathrm{d}Y_j}{\mathrm{d}r}) = 0. \tag{11}$$

Integrating and substituting Eqn. 10, an ODE for the mass fraction of species j is obtained:

$$\frac{\mathrm{d}Y_j}{\mathrm{d}r} - \frac{\dot{m}_{\mathrm{O}_2} + \dot{m}_{\mathrm{Fe}} + \dot{m}_{\mathrm{FeO}}}{4\pi\rho_{\mathrm{g}} D_j r^2} Y_j = -\frac{\dot{m}_j}{4\pi\rho_{\mathrm{g}} D_j r^2}. \tag{12}$$

An analytical solution to this first order ODE is found via the use of an integrating factor, and integrating both sides between $r = r_{\mathrm{p}}$ and the ambient gas phase region $r = \infty$ yields the following:

$$Y_{\infty,j} - Y_{\mathrm{p},j}\mathrm{Exp}\left[\frac{\dot{m}_{\mathrm{O}_2} + \dot{m}_{\mathrm{Fe}} + \dot{m}_{\mathrm{FeO}}}{4\pi\rho_{\mathrm{g}} D_j r_{\mathrm{p}}}\right] = \frac{\dot{m}_j}{\dot{m}_{\mathrm{O}_2} + \dot{m}_{\mathrm{Fe}} + \dot{m}_{\mathrm{FeO}}}(1 - \mathrm{Exp}\left[\frac{\dot{m}_{\mathrm{O}_2} + \dot{m}_{\mathrm{Fe}} + \dot{m}_{\mathrm{FeO}}}{4\pi\rho_{\mathrm{g}} D_j r_p}\right]). \tag{13}$$

The variable r'_{p} represents the adjusted particle radius, which takes into account the multi-species composition of the evaporating particle. For the equation describing O_2 transport, the entire particle surface is available for gas adsorption, hence, $r'_{\mathrm{p}} = r_{\mathrm{p}}$. For evaporating species j, the particle radius is scaled by the volume fraction of species j to the 2/3$^{\mathrm{rd}}$ power, i.e., $r'_{\mathrm{p}} = (\frac{V_j}{V_{\mathrm{p}}})^{\frac{2}{3}} r_{\mathrm{p}}$. This formulation captures the varying surface availability of Fe and FeO for evaporation as they are formed or consumed via reactions R1-R3. The mass fraction of gas-phase Fe and FeO in the bulk gas is assumed to be negligible. The

surface mass fraction of O_2 is zero under oxidizer-transport-limited combustion. Assuming phase equilibrium at the particle/gas interface, the partial pressures of gas-phase Fe and FeO at the particle surface can be determined via Clausius Clapeyron equations [9]. A uniform partial pressure of the inert gas (N_2) is assumed everywhere in the gas. LJ parameters for Fe [13] are used for the gas transport of FeO, due to the lack of literature on the parameters for FeO. The system of 3 coupled nonlinear equations is solved iteratively via the fsolve function on MATLAB.

3 Results and Discussion

The current model is compared to a typical temperature profile of a single laser-ignited iron particle [8] in Fig 3 (a). The particle first undergoes solid-phase ignition, where the combustion rate is initially limited by solid-phase oxidation kinetics. As the particle temperature increases and the combustion transitions into a external O_2 transport-limited regime, the phase change of FeO, Fe, and Fe_3O_4 are observed, represented by the flat temperature profiles at 1650 K, 1809 K, and 1870 K, respectively. The particle continues to burn in the external O_2 transport-limited regime until all Fe has been consumed at around 28 ms, reaching a temperature of about 2278 K. This is in good agreement with the peak temperature of the experimental curve of 2268 K, occurring at around 25 ms. The particle temperature then cools to the melting point of Fe_3O_4 (1870 K), through heat loss via convection and radiation. Fig 3 (b) and (c) show that the temperatures reached in these ambient gas conditions do not facilitate significant evaporation rates of Fe and FeO. In the time to particle burnout (28 ms), roughly 0.47% of the initial iron mass was evaporated. Convection has the most significant contribution to particle cooling (83%), followed by radiation (13%) and evaporation (4%). The deviation of the model after reaching the peak temperature suggests either an additional heat preserving effect (e.g. due to exothermic gas-phase reactions or a cloud of nanoparticles shielding the particle from heat loss to the bulk surroundings) or sustained heat release due to a kinetically controlled, slow further oxidation of the particle.

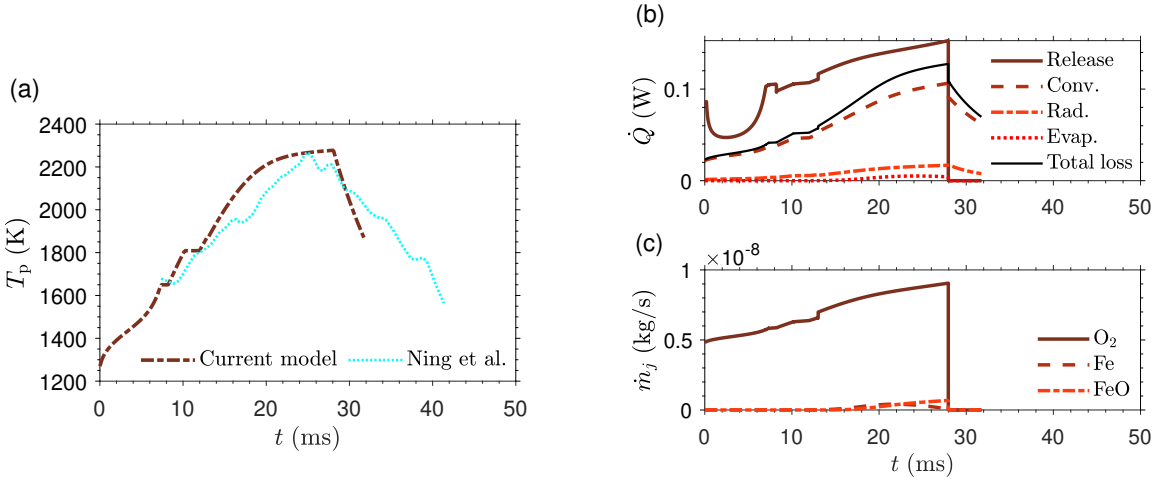

Figure 3: Left: (a) Time history of particle temperature predicted by the current model, compared to a typical smoothened temperature profile of a laser-ignited particle by Ning *et al.* [8] (dotted). Right: The time-evolution of rate of (b) heat release (solid), convective heat loss (dashed), radiative heat loss (dash-dotted), heat absorption due to evaporation (dotted), and total heat loss (thin solid), and (c) mass transport rate of gas-phase O_2 to the particle surface (solid), gas-phase Fe away from the particle surface (dashed), and gas-phase FeO away from the particle surface (dash-dotted). Initial particle diameter set to 54 μm, gas temperature set to $T_g = 300$ K, with $X_{O_2} : X_{N_2} = 0.21 : 0.79$.

4 Conclusion

An approximate zero-dimensional model for the liquid-phase combustion of a single iron particle was developed based on the simplifying assumption of external O_2 transport rate-controlled combustion. The formation of liquid-phase FeO was considered, as well as the evaporation of Fe and FeO and their inhibiting effect on O_2 transport to the particle surface. The model exhibited good agreement with the experimental temperature profile of a single laser-ignited particle. Possible sources of error to reconcile the discrepancy in the particle cooling rate prediction were discussed.

References

[1] J. Bergthorson, S. Goroshin, M. Soo, P. Julien, J. Palecka, D. Frost, D. Jarvis, Direct combustion of recyclable metal fuels for zero-carbon heat and power, Applied Energy 160 (2015) 368 – 382.

[2] J. Bergthorson, Recyclable metal fuels for clean and compact zero-carbon power, Progress in Energy and Combustion Science 68 (2018) 169 – 196.

[3] J. Païdassi, Sur la cinetique de l'oxydation du fer dans l'air dans l'intervalle 700-1250°C, Acta Metallurgica 6 (3) (1958) 184–194.

[4] X. Mi, A. Fujinawa, J. Bergthorson, A quantitative analysis of the ignition characteristics of fine iron particles, Combustion and Flame 240 (112011) (2022).

[5] P. Tóth, Y. Ögren, A. Sepman, P. Gren, H. Wiinikka, Combustion behavior of pulverized sponge iron as a recyclable electrofuel, Powder Technology 373 (2020) 210–219.

[6] D. Ning, Y. Shoshin, J. van Oijen, G. Finotello, L. de Goey, Burn time and combustion regime of laser-ignited single iron particle, Combustion and Flame 230 (2021) 111424.

[7] J. Huang, S. Li, W. Cai, Y. Qian, E. Berrocal, M. Aldén, Z. Li, Quantification of the size, 3d location and velocity of burning iron particles in premixed methane flames using high-speed digital in-line holography, Combustion and Flame 230 (2021) 111430.

[8] D. Ning, Y. Shoshin, M. van Stiphout, J. van Oijen, G. Finotello, P. de Goey, Temperature and phase transitions of laser-ignited single iron particle, Combustion and Flame 236 (2022) 421–432.

[9] W. Halstead, A review of saturated vapour pressures and allied data for the principal corrosion products of iron, chromium, nickel and cobalt in flue gases, Corrosion Science 15 (6-12) (1975) 603–625.

[10] B. McBride, Coefficients for calculating thermodynamic and transport properties of individual species, Vol. 4513, NASA Langley Research Center, 1993.

[11] M. Muller, H. El-Rabii, R. Fabbro, Liquid phase combustion of iron in an oxygen atmosphere, Journal of Materials Science 50 (9) (2015) 3337–3350.

[12] G. Burgess, R. Waltenberg, The Emissivity of Metals and Oxides: Measurements with the micropyrometer, Vol. 11, US Department of Commerce, Bureau of Standards, 1915.

[13] A. Arkundato, Z. Su'ud, S. Sudarko, M. Hasan, M. Celino, Molecular dynamics simulation of corrosion mitigation of iron in lead-bismuth eutectic using nitrogen as corrosion inhibitor, in: Journal of Physics Conference Series, 2015.